buildings

MDPI

Review

Enhancing Performance of Engineering Structures under Dynamic Disasters with ECC–FRP Composites: A Review at Material and Member Levels

Debo Zhao [1,2,3], Bin Chen [1,2,3] and Jingming Sun [4,5,*]

1 College of Civil and Transportation Engineering, Shenzhen University, Shenzhen 518061, China; debozho@szu.edu.cn (D.Z.); 2210474051@email.szu.edu.cn (B.C.)
2 Key Laboratory for Resilient Infrastructures of Coastal Cities (MOE), Shenzhen University, Shenzhen 518060, China
3 Shenzhen Key Laboratory of Green, Efficient and Intelligent Construction of Underground Metro Station, Shenzhen 518060, China
4 College of Civil Engineering, Hunan University, Changsha 410082, China
5 Hunan Provincial Key Lab on Damage Diagnosis for Engineering Structures, Hunan University, Changsha 410082, China
* Correspondence: sunjingming@hnu.edu.cn

Abstract: Dynamic loadings arising from impact, explosive, and seismic disasters impose high requirements on the performance of engineering structures during service periods. Engineered cementitious composite (ECC) exhibits exceptional toughness and crack resistance, while fiber-reinforced polymer (FRP) possesses lightweight and high-strength properties. ECC and FRP composites show promising potential in enhancing the resilience of existing structures under dynamic disaster scenarios. However, most research on ECC and FRP has primarily focused on static properties, while investigations of dynamic properties are limited. This paper provides a comprehensive review of the dynamic properties of ECC and FRP composites followed by a summary of studies conducted on the dynamic behavior of ECC and FRP strengthened members, which provides valuable insights for further research on these materials and their applications in strengthening structures under dynamic disasters.

Keywords: ECC; FRP; ECC–FRP grid composites; strengthen; dynamic loading

check for updates

Citation: Zhao, D.; Chen, B.; Sun, J. Enhancing Performance of Engineering Structures under Dynamic Disasters with ECC–FRP Composites: A Review at Material and Member Levels. *Buildings* **2023**, *13*, 2099. https://doi.org/10.3390/buildings13082099

Academic Editor: Antonio Caggiano

Received: 30 June 2023
Revised: 11 August 2023
Accepted: 17 August 2023
Published: 18 August 2023

Copyright: © 2023 by the authors. Licensee MDPI, Basel, Switzerland. This article is an open access article distributed under the terms and conditions of the Creative Commons Attribution (CC BY) license (https://creativecommons.org/licenses/by/4.0/).

1. Introduction

During the service period, there are high risks for engineering structures suffering from extreme loading caused by various kinds of natural and man-made dynamic disasters, such as impacts, explosions, and earthquakes [1,2]. The severe damage to structures in these cases often induces serious casualties, enormous economic losses, and devastating social impacts [3,4]. Therefore, there is an urgent need for high-performance building materials that can enhance structural resilience under extreme dynamic disasters. Typically, structural members subjected to impact and explosive loads experience high peak forces and short durations. Consequently, enhancing the ductility of these components to dissipate impact energy proves to be a more practical and economical approach compared to merely increasing the stiffness and resistance of entire structures, in most cases [5]. Correspondingly, at the material level, there has been a strong emphasis on improving the toughness and deformation capacity of building materials.

Engineered cementitious composite (ECC) is a highly promising building material used in the construction, strengthening, and rehabilitation of structures under dynamic disasters, primarily due to its outstanding crack control capability and high toughness [6]. ECC is created by incorporating high-performance fibers, such as polymer fibers or metal fibers, into the cementitious matrix, which grants it the ability to exhibit tensile strain-hardening

and multiple cracking properties. The excellent toughness and cracking resistance properties of ECC [7] enable it to effectively absorb inputted energy and distribute stresses, thereby protecting the structure from severe local damage caused by dynamic loadings, such as spalling, scabbing, and perforation [8–10]. Strain-hardening cementitious composites (SHCC), ultra-high toughness cementitious composites (UHTCC), ultra-high ductility cementitious composites (UHDCC), and ultra-high ductility concrete (UHDC) can all be referred to as ECC. By carefully adjusting the proportions, dimensions, and types of fibers, ECC can exhibit excellent strength and ductility properties, even at high strain rates [11,12].

Fiber-reinforced polymer (FRP) is another extensively used building material in structural strengthening due to its high strength, corrosion resistance, and ease of construction and transportation. It has been demonstrated that strengthening reinforced concrete (RC) members with FRP can enhance impact resistance to a certain extent [13]. However, the commonly employed FRP strengthening methods, such as external bonding and near-surface mounting, typically utilize epoxy resin as the concrete–FRP interface binder, which deteriorates over time due to the natural aging of organic adhesives. This degradation leads to durability issues and limits the service life of the strengthened system [14,15]. Additionally, the FRP–concrete interface is relatively weak compared to the high-strength FRP, often resulting in premature failure of the FRP strengthening system due to the debonding of the FRP–concrete interface, especially under dynamic loading conditions [16]. The dynamic loadings demand high deformation capacities of structural members, which may make damage to the FRP–concrete interface more apparent, significantly reducing the utilization efficiency of FRP strengthening materials [17,18].

In recent years, a new technology for strengthening structures has emerged, combining FRP and ECC. This innovative approach leverages the strengths of both materials, resulting in improved performance and overcoming the limitations of using single materials [19–21]. In this technique, ECC is employed as an inorganic adhesive, replacing epoxy resin, while FRP grids are embedded within the ECC to enhance bonding and collaborative capabilities [19–21]. The combined strengthening system has exhibited excellent performance under static conditions [19,22–25]. The multi-crack development characteristic of ECC plays a crucial role in avoiding stress concentration typically observed with a single crack at traditional bonding interfaces. This feature significantly enhances the bonding performance at the interface [21]. Building on this success, researchers have explored the application of ECC–FRP combination strengthening technology in the dynamic strengthening domain. Preliminary investigations have shown promising results, demonstrating the effectiveness of this technology in enhancing the performance of reinforced concrete (RC) members under dynamic loading [26–29]. However, a comprehensive understanding of the strengthening mechanisms has not been reached.

This paper provides a comprehensive review of the existing literature on ECC and FRP-reinforced ECC technologies under dynamic loadings, focusing on both material and member aspects. The following is an overview of the key topics covered in the review: Firstly, the dynamic properties of ECC and FRP-reinforced ECC materials are discussed, including their damage mode, dynamic strength, and energy dissipation capacity. Additionally, the paper delves into the critical factors that influence the dynamic behaviors of these materials. Subsequently, the research progress on the dynamic behaviors of ECC members, and members strengthened by ECC, FRP, or ECC–FRP composite layers under dynamic loading is summarized and compared.

2. Dynamic Mechanical Properties of ECC + FRP Composites

2.1. Dynamic Mechanical Properties of ECC

Engineered cementitious composite (ECC) has attracted much attention due to its outstanding toughness properties. The dynamic loading behavior of ECC under high strain rates has been a research focus. For different strain rates, compressive and tensile properties of ECC exhibit significant strain-rate sensitivity, and key influencing factors have been identified and investigated, such as fiber type, fiber content, fiber size, and matrix mix

proportion [30–48]. Table 1 provides comprehensive details of compressive and tensile experiments of ECC.

Numerous researchers have investigated the compression behavior of ECC under dynamic compression loading at different strain rates [30–36]. Under high strain rates, the dynamic compression behavior of ECC can be divided into three main stages: (1) Elastic stage—in this stage, the stress–strain relationship of ECC increases approximately linearly. (2) Strain-hardening stage—as the strain continues to increase, the rate of stress growth slows down, and microcracks begin to increase and develop in the material. (3) Damage softening stage—after reaching the peak stress, internal cracks begin to expand and the strength of the ECC specimen decreases sharply until it is damaged. Experimental results indicate that the dynamic compression strength, dynamic increase factor of compression (DIFc), and energy absorption capacity of ECC exhibit a positive correlation with increasing strain rates within the range of 30 to 400 s^{-1} [30–36], exhibiting clear strain-rate sensitivity. Figure 1 shows the compressive stress–strain curves at different strain rates. In addition, the increase in strain rate leads to more fracture damage to the fibers. In the various studies, three failure mechanisms of the bond between the fibers and the cement mortar can be summarized as follows: (1) When the bond between the two is strong while the strength of the cement mortar is low, failure occurs due to damage in the mortar near the fiber–matrix interface; (2) when the bond between the fibers and the cement mortar is weak, the fibers directly pull out from the mortar; and (3) if the bond between the fibers and the matrix is sufficiently strong, the fibers fail by fracturing at the cracking location of the matrix [30–48]. Under dynamic compression loading, the failure mode varies with different fiber types. For example, when ECC contains a combination of polyvinyl alcohol (PVA) fibers and steel fibers, the steel fibers exhibit a lower tendency to fracture due to their higher strength and smoother surface characteristics [30,31]. On the other hand, when PE fibers are mixed with steel fibers in ECC, the high content of polyethylene (PE) fibers can hinder large deformation and the formation of large cracks in the specimen, thereby inhibiting steel fiber fracture [34].

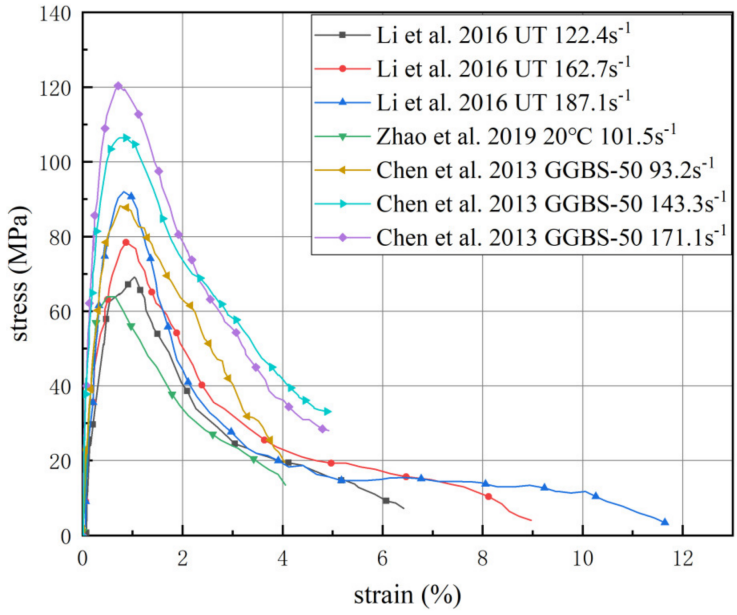


Figure 1. Compressive stress–strain curves under different strain rates [30,31,33].

Direct tensile and splitting tensile tests under dynamic tensile loading reveal that the tensile properties of ECC exhibit similar strain-rate sensitivities as the compression behavior. Figure 2 presents the tensile stress–strain curves at different strain rates. In most cases, the ultimate strain of ECC generally decreases with strain rate in the low strain-rate range ($\leq$0.1 s^{-1}) [37,39,40,44]. However, some researchers have reported insignificant

changes in strain capacity with strain rate [41]. As the strain rate continues to increase (>0.1 s^{-1}), the strain capacity of ECC begins to increase as well [37,42]. Moreover, both the dynamic tensile strength and energy absorption capacity of ECC exhibit an increasing trend with strain rate, regardless of whether the strain rate is low or high [37–47]. The sensitivity of ECC to strain rate is stronger when compared to normal concrete [41]. From a microscopic perspective, higher strain rates increase the likelihood of fiber breakage during tension [37,39]. In addition, Yang et al. [44] have indicated that the stiffness and strength of the fibers, the toughness of the matrix, and the strength of the fiber–matrix interface all exhibit strain-rate sensitivity, which increases with increasing strain rate.

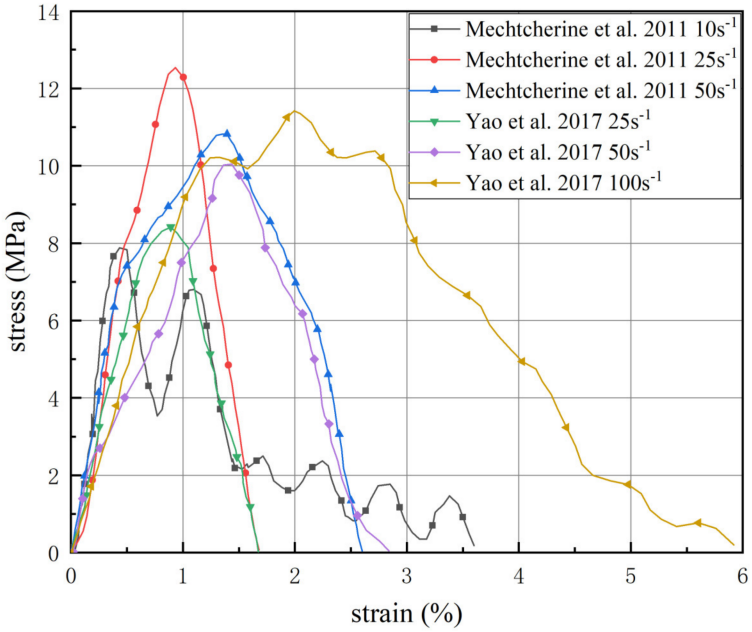


Figure 2. Tensile stress–strain curves under different strain rates [37,42].

The strain-rate effects of ECC have been influenced obviously by fiber type and matrix mix proportion. Curosu et al. [38,48] discovered that a more homogeneous microstructure of the high-strength matrix results in higher brittleness and lower strain-rate sensitivity. The fiber–matrix bond in PVA–ECC leads to a reduction in initial crack strength and strain-softening behavior of the material at high strain rates, while the high-density polyethylene (HDPE) fiber and cement matrix frictional interaction results in significant dynamic strengthening. Furthermore, the strain-rate sensitivity of UHTCC has been found to be influenced by the presence of free water within the material. Under the same impact air pressure of the split Hopkinson pressure bar (SHPB) system, the dynamic tensile strain rate of water-absorbing saturated UHTCC was 25–41% lower compared to dry UHTCC. This reduction in strain rate is likely attributed to the viscous effect of free water, which restricts the deformation of the specimen. Additionally, it was observed that the strain rate of saturated ECC decreased even more significantly than that of dry ECC as the impact pressure increased [43].

Table 1. Details of ECC compressive and tensile experiments.

Reference	Method of Test	Specimen Size (mm)	Type and Content of Fibers	Other Parameters	28 Days Quasi-Static Compressive Strength (MPa)	28 Days Quasi-Static Tensile Strength (MPa)	Dynamic Loading		The Highest Dynamic Strength (MPa)	The Highest DIF [8]
							Strain Rates (Actual)	SHPB Air Pressure (MPa)		
Li et al. [30]	Dynamic compressive 80 mm SHPB bar	Φ70 × 35 cylinder	0~1.5%SF [1] + 2%PVA	/	55.9~58.1 (70.7 mm cubes)	/	118.0/s~188.0/s (113.8/s~192.1/s)	0.6~1.1	105+ in 184/s and 1.5%SF	1.5+ in 184/s and 1.5%SF
Zhao et al. [31]	Dynamic compressive 80 mm SHPB bar	Φ68 × 35 cylinder	1.5%SF + 2%PVA	Temperature 20 °C~800 °C	55.5 (20 °C) (Φ68 × 140 cylinder)	/	30/s~150/s (17.2/s~142.0/s)	/	69.8 in 142/s (20 °C)	1.26 in 142/s (20 °C)
Kai et al. [32]	Dynamic compressive 100 mm SHPB bar	Φ98 × 50 cylinder	2%PVA	Water ratio + Superplasticizer ratio 0.40~0.44 + 0.013~0.015	72.9~74.0 (70.7 mm cubes)	/	(96/s~197/s)	0.9~1.5	164.41 in 191/s and 0.42 + 0.014	2.22 in 191/s and 0.42 + 0.014
Chen et al. [33]	Dynamic compressive 40 mm SHPB bar	Φ38 × 20 cylinder	2%PVA	The ratio of cement replaced with ground granulated blast furnace slag (GGBS) 0.5~0.8	50+~73 (70.7 × 70.7 × 220 mm^3 prism)	3.65~5.38 (12 × 40 × 160 mm^3 prism)	90/s~180/s (84.8/s~184.6/s)	/	120 in 171.1/s and 50% GGBS	1.65+ in 171.1/s and 50% GGBS
Wang et al. [34]	Dynamic compressive 80 mm SHPB bar	Φ77 × 38 cylinder	2%PVA 0.5%SF + 1.5%PE [3]	Silica fume was used in the SHCC–SF + PE to replace 10% of cement	64.5 (Φ77 × 38 cylinder) 83.8	/	30~300/s (84/s~307/s)	/	140+ in 307/s and SHCC–SF + PE	1.8+ in SHCC–PVA
Zhang et al. [35]	Dynamic compressive 50 mm SHPB bar	Φ48 × 25 cylinder	0~0.3%BF [4] + 0~1%SF	/	30.2~34.1 (Φ48 × 25 cylinder)	3.24~4.13 (80 mm × 30 mm × 12.7 mm dumbbell specimen)	(36.1/s~202.3/s)	0.2~0.56	63.0 in 182.9/s and 2%BF + 1%SF	1.85 in 182.9/s and 2%BF + 1%SF
Chen et al. [36]	Dynamic compressive 40 mm SHPB bar	Φ37 × 22 cylinder	2%PVA	Content of Fly ash 0.5~0.8	25+~57.9 (40 × 40 × 160 mm^3 prism)		200/s~400/s (165/s~399/s)	/	78.00 in 386/s and 50% fly ash	1.581 in 399/s and 70% fly ash
Mechtcherine et al. [37]	Uniaxial direct dynamic tensile High-rate MTS test machine	100 mm × 40 mm × 24 mm dumbbell specimen	2.2%PVA	/	/	4.54~5.51 (100 mm × 40 mm × 24 mm dumbbell specimen)	0.00001/s~50/s	/	12.08 in 25/s	2.5+ in 25/s
Curosu et al. [38]	Uniaxial direct dynamic tensile Modified Hopkinson bar	Φ20 × 50 cylinder Φ20 × 25 cylinder	2%PVA 2.06%HDPE [5]	/ Two strengths of HDPE–SHCC Normal/High strength	/	3.8 (Φ20 × 50 cylinder) 5.3 (Φ20 × 25 cylinder) 3.6 (Φ20 × 50 cylinder) 6.5 (Φ20 × 50 cylinder) 8.5 (Φ20 × 25 cylinder)	100/s (Φ20 × 50 cylinder) 200/s (Φ20 × 25 cylinder)	/	12.8 in 200/s and High strength HDPE–SHCC	2.8 in 100/s and Normal strength HDPE–SHCC
Yu et al. [39]	Uniaxial direct dynamic tensile	80 mm × 30 mm × 12 mm dumbbell specimen	20 kg/m^3 PE	Length-to-diameter ratio 500~900	149 (50 mm cubes)	11.03~17.40 in 0.0001/s	0.0001/s~0.05/s	/	18.88 in 0.01/s and UHP-ECC-900	/
Ranade et al. [40]	Uniaxial direct dynamic tensile	Gauge length 90 mm dogbone specimen	19 kg/m^3 PE	/	/	14.5 in 0.0001/s	0.0001/s~10/s	/	20.6 in 10/s	/
Maalej et al. [41]	Uniaxial direct dynamic tensile	300 × 75 × 15 mm^3 prism	0.5%SF + 1.5%PE	/	70 (50 mm cubes) 55 (Φ100 × 200 cylinder)	3.1 (300 × 75 × 15 mm^3 prism)	2×10^6/s~0.1/s	/	6.5+ in 0.1/s	2.0+ in 0.1/s
Yao et al. [42]	Uniaxial direct dynamic tensile High-rate MTS test machine	150 × 25 × 10 mm^3 prism	2.2%PVA	/	/	/	25/s~100/s	/	9.9 in 100/s	/
Zhao et al. [43]	Dynamic splitting tensile SHPB	Φ68 × 35 cylinder	2%PVA	Free water content Dry/Saturated specimens	/	6.0 (Dry/Splitting tensile) 4.6 (Saturated/Splitting tensile)	(Dry: 3.0/s~3.9/s Saturated: 4.0/s~6.6/s)	0.3~0.5	10.2 in 6.6/s and dry specimen	1.7 in 6.6/s and dry specimen

Table 1. *Cont.*

Reference	Method of Test	Specimen Size (mm)	Type and Content of Fibers	Other Parameters	28 Days Quasi-Static Compressive Strength (MPa)	28 Days Quasi-Static Tensile Strength (MPa)	Dynamic Loading		The Highest Dynamic Strength (MPa)	The Highest DIF [8]
							Strain Rates (Actual)	SHPB Air Pressure (MPa)		
Zhao et al. [45]	Dynamic splitting tensile 80 mm SHPB bar	Φ68 × 34 cylinder	0~1.5%SF + 2%PVA	/	46.8~54.6 (Φ68 × 34 cylinder)	8.16~10.12 (Splitting tensile)	(1.2/s~11.0/s)	0.3~0.7	16.4 in 9.9/s and 1.5%SF + 2%PVA	1.84 in 10.1/s and 0%SF + 2%PVA
Chen et al. [46]	Dynamic splitting tensile 100 mm SHPB bar	Φ100 × 50 cylinder	2%PVA	Temperature 20 °C–800 °C	/	9.23 (20 °C, Splitting tensile)	4.5/s~10.5/s (4.34/s~10.95/s)	/	22.94 in 10.95/s (20 °C)	2.49 in 10.95/s (20 °C)
Yang et al. [47]	Dynamic splitting tensile 100 mm SHPB bar	Φ50 × 25 cylinder	0~3%PVA	/	/	/	/	0.11~0.2	13.5+ in 0.18 Mpa and 1.5%PVA	/
Curosu et al. [48]	Uniaxial direct dynamic tensile	100 mm × 40 mm × 24 mm dumbbell specimen	2%HDPE	/	133.5 (100 mm cubes)	7.6	0.0005/s	/	/	/
			2%Aramid		144.8 (100 mm cubes)	9.4				
			2%PBO-AS [6]		140.3 (100 mm cubes)	9.8				
			2%PBO-HM [7]		142.9 (100 mm cubes)	8.4				

[1] SF: steel fiber; [2] PVA: polyvinyl alcohol; [3] PE: polyethylene; [4] BF: basalt fiber; [5] HDPE: high density polyethylene; [6] PBO-AS: P-phenylene-2,6-benzobisoxazole as-spun; [7] PBO-HM: P-phenylene-2,6-benzobisoxazole high-modulus; [8] DIF: dynamic increase factor.

The dynamic tensile properties of ECC are also influenced by the type, content, and dimensions of fibers used. Commonly used fibers in ECC include PVA fiber, PE fiber, and polypropylene (PP) fiber. Meanwhile, steel fiber has also been studied by some researchers [41,45]. Yang et al. [47] conducted dynamic splitting tensile tests on ECC specimens with varying PVA volume content from 0% to 3%. The results indicated that the splitting tensile performance of ECC improved with increasing PVA fiber content within the range of 0% to 1.5%. The splitting strength can be increased by up to 90.7% compared to the specimen without PVA fibers. However, beyond this range, the peak splitting stress started to decrease, suggesting that the large volume fraction of PVA fibers reduces the strength of the ECC material. The phenomenon could be attributed to the fact that within a certain content range, increasing fiber content enhances the ability of ECC to limit crack development due to the bridging effect of the fibers. However, when the fiber content is higher, the strength of the concrete will decrease. In addition, with the increase in fiber content, the spacing between the fibers decreases, which may lead to knots and agglomeration of the fibers, affecting the role of the fibers in enhancing toughness and limiting cracks. Furthermore, Zhao et al. [45] demonstrated that adding steel fibers to UHTCC with 2% PVA fibers was also effective in improving the dynamic splitting tensile properties. Within the range of 0 to 1.5% volume of steel fibers, performance improves as steel fiber content increases, but the degree of steel fiber contribution to the tensile properties of UHTCC was affected by the strain rate. A study conducted by Yu et al. [39] indicated that a higher fiber length-to-diameter ratio (L:D) increased the number of cracks and reduced the width and spacing of cracks, which is beneficial for the bridging effects of the fibers. Moreover, pullout was more likely to occur for fibers with a smaller L:D ratio, while for fibers with a larger L:D ratio, the fibers were prone to rupture. From the parameters of the fibers in that study, it may be concluded higher lengths lead to higher embedment areas and increased forces, and lower diameters have lower fiber stiffness and are more prone to rupture.

Several researchers have investigated the self-healing capacity of ECC after experiencing dynamic loading. Self-healing of concrete consists of two main aspects, the first is autogenous healing, which consists of three main parts: (1) the physical process: calcium silicate hydrate absorbs water and expands to narrow the cracks; (2) the chemical process: products of continued hydration of unhydrated cement as well as calcium carbonate generated by the reaction of Ca^{2+} in the concrete with $CO_3{}^{2-}$ in the water in the cracks precipitates on the surface of the cracks to narrow the cracks; (3) fine particles from the cracking process and water plugging the cracks. These three parts have calcium carbonate precipitation as the most significant healing factor. It is noteworthy that the use of ECC to reduce the width of the crack is also a type of autogenous healing. The second aspect is autonomous healing, which employs either encapsulation or vascular systems to deliver healing agents into the cracks, or immobilization, where organic compounds and microorganisms are embedded in inorganic matrices by various methods and restricted from moving to ensure that the healing action works properly. In self-healing concrete, the main healing agents used are mineral admixtures, bacteria, and adhesives [49–51]. Guo et al. [52] conducted a study using drop hammer impact to induce cracks in SHCC specimens doped with MgO-type expansive agent (MEA). These specimens were then exposed to various environments, including water, seawater, saturated $Ca(OH)_2$ solution, and 3% NaCl solution. The failure criterion for the specimens was set as a maximum crack width larger than 200 μm. Their findings revealed that after 120 days of self-healing following damage from drop hammer impact loading, the SHCC required more impacts to reach failure again. Notably, the specimens in the seawater environment showed the largest increase in the number of impacts. This observation was attributed to the fact that the repaired SHCC specimens not only have the repaired cracks cracked again, but also new cracks appeared, which further dissipated impact energy. Tang et al. [53] made advancements in ordinary SHCC by introducing reactive MgO and quicklime as mineral substitutes (MS) and incorporating triethanolamine (TEA) additives into the high-volume

fly ash matrix. They applied dynamic reversed-cyclic (DRC) preloading in their experiments. The study demonstrated that the modulus of rupture after healing of the preloaded cracks could approach or even exceed that of the unloaded control. This was due to the more effective self-healing produced by the cracks compared to the further hydration of the specimen concerning the bond strength between fibers and the matrix. Furthermore, the specimens with MS and TEA showed superior healing performance under DRC reloading compared to those without MS and TEA. The modulus of fracture, first crack strength, and flexural stiffness also exhibited significant improvements compared to the DRC preload. These enhancements were attributed to the continuous hydration of the specimens and the fact that MS could further improve healing efficiency through the hydration and expansion reactions of MgO and quicklime.

In general, understanding the behavior of ECC under dynamic loading is crucial for design and application in fields such as impact and seismic resistance. However, the mechanical behaviors of ECC under different dynamic loadings still need further research to improve the reliability and effectiveness of its application.

2.2. Static Properties of ECC–FRP Grid Composites

Although ECC exhibits much higher tensile toughness than normal concrete, its tensile strength is comparable to that of normal concrete. Considering scenarios involving impact or seismic events that demand both toughness and strength, researchers have explored ECC–FRP grid composites. These composites can achieve a highly collaborative effect in terms of tensile strength, toughness, energy dissipation, and crack control [25]. The common approach involves embedding FRP grids into ECC, where ECC can provide excellent crack resistance and compressive strength, and FRP contributes a high tensile property and stiffness to the material. Numerous studies have demonstrated that the tensile performance of the composite material with embedded FRP grids is significantly improved compared to the tensile strength of unembedded ECC [23–25,54], as depicted in Figure 3 (experimental date from ref. [55]). However, the ultimate tensile strain remains inconclusive across various research studies.

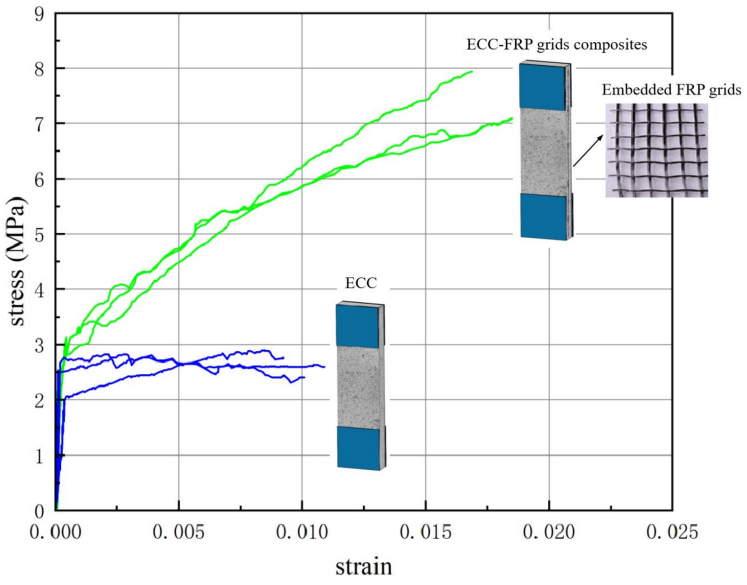


Figure 3. Uniaxial tensile stress–strain curve of ECC–FRP grid composites and ECC (Experimental data from [55]).

As one of the main materials of composite materials, the type and properties of FRP have a significant impact on the performance of composites. Zhu et al. [22] conducted uniaxial tensile tests on ECC specimens reinforced with Carbon Fiber-Reinforced Polymer (CFRP) grids. The test results indicated that the addition of CFRP grids enhanced the

tensile strength and ultimate tensile strain of ECC. The failure mode of the specimens was characterized by FRP grid rupture, and the specimens exhibited multiple cracks as well as high toughness due to the properties of ECC. The PVA fibers were observed to be pulled out from the fracture location. However, the ultimate tensile strain of the CFRP grid in the composite was only 52% of its own tensile strain and was independent of the number of layers of the grid in the specimen. Zheng et al. [23] conducted tensile tests on UHTCC specimens reinforced with Basalt Fiber-Reinforced Polymer (BFRP) grids. The failure mode was similar to that of the CFRP grids reinforced ECC, ending with BFRP rupture and PVA fiber pullout or rupture. During the damage process, the number of transverse microcracks on the specimen surface increased significantly with the reinforcement ratio of BFRP grids, and the average spacing and width decreased. The tensile strength of the specimen decreases slightly as the water/cement ratio of the matrix (i.e., UHTCC) increased. Meanwhile, the axial stiffness, tensile strength, and ultimate tensile strain of the composite specimens were increased considerably. Deng et al. [54] compared the effect of CFRP grids and BFRP grids on the tensile strength of the composite materials and found that the CFRP grids had a greater increase in tensile strength compared to the BFRP grids. In addition, the enhancement of tensile properties by FRP grids was insignificant before the specimens reached cracking strength. After cracking, the FRP grids acted as the primary loading component to withstand the tensile stress.

Similarly, the choice of fiber type in ECC has a significant effect on the performance of the composites. All studies in the last paragraph focused on the PVA–ECC matrix. The stress–strain curve can generally be divided into two stages: the elastic stage and the multi-crack development stage. The composite material enters the second stage after the cracking of ECC. In this stage, the cracks start to increase and develop until the specimen is pulled off and broken, which can be simplified as in Figure 4. Li et al. [24] utilized three different weaves of BFRP grids to embed UHDCC (PE fibers). The authors found that the stress–strain curve was different from the study of Deng et al. [54]. After undergoing the elastic stage and multi-crack development stage, there were two different development patterns according to the volume ratio of the added BFRP grids. When the grid volume ratio was greater than 1%, the tensile stress decreased sharply in the third stage, and progressive ruptures of fiber rupture occurred, but a larger crack had not yet been observed. Until the sudden rupture of FRP, the material enters the fourth stage, when the stress is relatively stable and the strain continues to increase until finally the PE fibers rupture or pull out, and part of the woven threads of FRP also pulled out, forming a large crack and entering the softening stage before failure (Figure 5a). On the other hand, when the volume ratio of the FRP grid was less than 1%, the reinforcement degree was not high in the second stage. After the end parts of the FRP woven threads ruptured, the stress–strain curve directly entered the stress stabilization stage, finally forming a large crack and entering the softening stage before failure (Figure 5b). Gong et al. [25] wrapped styrene-butadiene impregnation yarns and polyacrylate impregnation yarns on CFRP, respectively. The PE-SHCC and as-spun poly(p-phenylene-2,6-benzobisoxazole) (PBO-AS) fibers SHCC (PBO-AS-SHCC) were then strengthened with these two CFRPs, both grids having a volume ratio of 2%. The stress–strain curve close to that of Figure 5a was also observed on the specimens with lower strength CFRP grid-reinforced PE-SHCC, while the two-stage curve of Figure 4 was still observed when the CFRP grid strength was higher. Therefore, it can be concluded that the tensile stress–strain curve of the composite material may be related to the toughness of the fibers, the interfacial bonding performance with the matrix, and the bridging performance. When the FRP gradually ruptures and fails, if the fibers in the ECC have not completely ruptured or been pulled out, the ECC still has the capability to bear the tensile stress, and the strain-hardening behavior is observed in the form of platform segments on the curve.

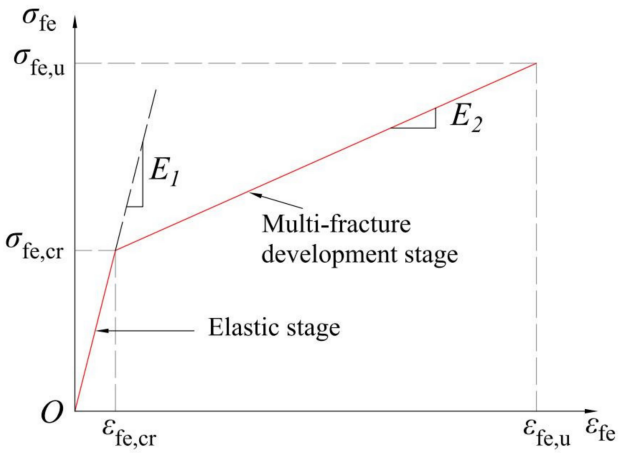


Figure 4. Uniaxial tensile stress–strain curve model for ECC–FRP grid composites [54].

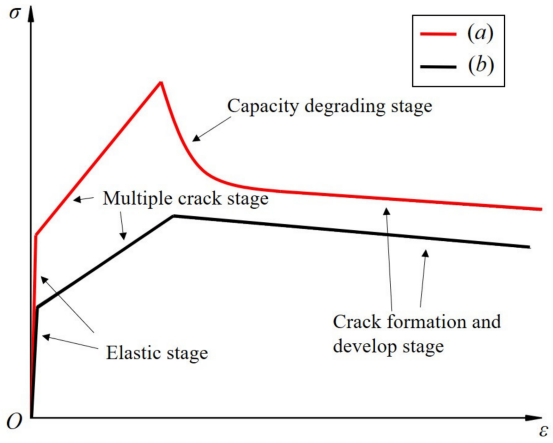


Figure 5. Uniaxial tensile stress–strain curve model of UHDCC–BFRP grid composites (Experimental data from [24]).

The bonding performance between the grids and the matrix is also a crucial factor influencing the composite material. Jiang et al. [19] conducted pull-out tests on BFRP grids embedded in UHDCC to investigate the influence of grid size, aspect ratio, and embedment length on the bonding performance between the grids and the matrix. The test results indicated that the bond strength decreased with the increase in embedment length. In addition, the effect of grid size on bond strength was related to the size of short fibers in UHDCC. When the fiber length is shorter than the grid width, the fiber could pass through the grid, resulting in higher bond strength. Deng et al. [56] studied the bonding performance of BFRP grids with ECC. They found that the bonding performance of FRP grids with ECC also increased with the increase in FRP thickness and ECC layer strength. Additionally, sand adhesion on the surface of FRP grids contributed to an improvement in the bonding force.

In conclusion, ECC and FRP grids demonstrate excellent cooperative performance under static loading, offering superior tensile properties, toughness, and crack control compared to individual materials. When used to strengthen RC structures, ECC–FRP grid composites can enhance the overall load-bearing and energy-absorption capacities of the structure, showing promising application prospects. However, there is a scarcity of research on the mechanical properties of ECC–FRP grid composites under dynamic loading. Further research and practical experience are required to improve the design and application of this composite material in dynamic scenarios.

3. Dynamic Performance of ECC Members and ECC-Enhanced Members

3.1. Dynamic Performance of ECC Members

Many studies have provided evidence that ECC members exhibit superior ductility, energy absorption capacity, and impact resistance compared to ordinary mortar or concrete members.

For reinforced ECC members, ECC demonstrates an excellent cooperative performance with the reinforcements. The high toughness of ECC enables it to deform well with the reinforcements, causing plastic yielding of longer reinforcement segments [11]. This characteristic further helps prevent the formation and propagation of cracks. In the case of multiple impacts at low energy, ECC demonstrates the delayed generation of cracks and well-distributed microcracks, and no individual or multiple large cracks were crossing the specimen leading to failure [11,12,57]. Moreover, ECC slabs did not present severe peeling or fragmentation, had a stronger deformation capacity, and withstood more impacts before failure [11,12,57,58]. The mechanism underlying the phenomena is that the well-distributed microcracks in the ECC slabs allow for a large volume of ECC to participate in the absorption of impact energy while maintaining structural integrity [12].

Unreinforced ECC members also exhibit excellent deformability and energy absorption [42,59–63]. Ranade et al. [59] compared the impact resistance of high strength-high ductility concrete (HSHDC) slabs and fiber-reinforced ultra-high performance concrete (FR-UHPC) slabs with compressive strengths of 166 MPa and 201 MPa, respectively. HSHDC also exhibits better impact resistance due to its high ductility, multiple microcracks, and high energy absorption capacity [59]. Meanwhile, Qi et al. [62] studied the impact damage of PVA–ECC beams under low-velocity impact loading using polyvinylidene fluoride (PVDF) thin-film sensors and piezoceramic-based smart aggregate and found that PVA–ECC beams exhibited an impact bouncing effect, where the shot-ball made contact with the beam twice in a single drop impact test. This bouncing effect gradually decreased with the increase and development of cracks under multiple impacts until it disappeared.

The material proportions of ECC have an effect on the impact resistance of ECC members. Yıldırım et al. [60] conducted a study comparing fly ash and blast furnace slag at different dosage levels. Their findings revealed that blast furnace slag specimens exhibited smaller residual mid-span deflection, indicating better impact resistance when compared to fly ash specimens. Furthermore, the impact resistance of the specimens was found to decrease significantly with an increase in volcanic ash content. Notably, fly ash specimens showed a greater reduction in impact resistance compared to blast furnace slag specimens. In one study, Zhang et al. [61] investigated the effects of adding rubber crumbs to PVA–ECC, partially replacing silica sand. The inclusion of rubber crumbs resulted in enhanced ductility, multiple microcrack properties, and an impact-bouncing effect in the ECC beams. As a consequence, the ECC beams demonstrated improved damage tolerance and energy absorption capacity.

Several researchers have explored the possibility of finding more cost-effective fibers that offer excellent performance in ECC, serving as alternatives to PVA fibers, particularly for dynamic loading conditions. Yıldırım et al. [60] compared the impact resistance of PVA–ECC and nylon fiber–ECC and found that although the improvement in impact resistance for ECC beams with nylon fibers was not as substantial as with PVA fibers at the same volume content, it still showed a considerable strengthening. Through appropriate adjustments in ECC proportions, nylon fiber–ECC members could achieve impact resistance comparable to their PVA–ECC counterparts. In another study conducted by Lu et al. [63], three types of fiber-reinforced SHCC were compared: polyethylene terephthalate SHCC (PET–SHCC), PVA–SHCC, and a hybrid fiber SHCC. The researchers found that SHCC with 1% PVA and 1% PET hybrid fibers and SHCC with 2% PVA fiber exhibited similar capacity to absorb energy under impact loading.

3.2. Dynamic Performance of ECC + FRP Enhanced Members

Regarding the application of engineered cementitious composites (ECC) and fiber reinforced polymer (FRP) in strengthening, three main types of strengthening systems can be identified: (1) Strengthening the member using ECC alone (Figure 6a); (2) strengthening the member using FRP alone (Figure 6b); (3) strengthening the member using an ECC–FRP composite system (Figure 6c).

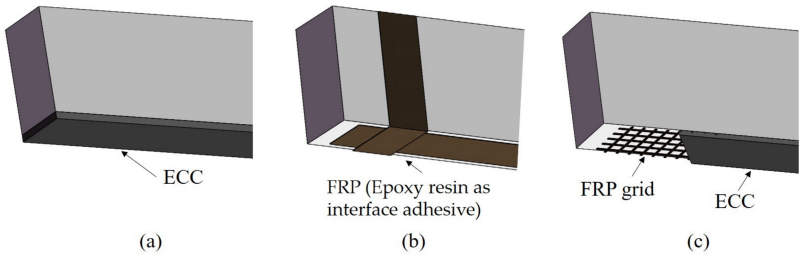


Figure 6. Three strengthening systems: (**a**) member strengthened with ECC; (**b**) member strengthened with FRP; (**c**) member strengthened with ECC–FRP.

3.2.1. Dynamic Performance of ECC Enhanced Members

In recent years, members strengthened with an ECC layer have been extended to the dynamic field to satisfy the requirements of engineering structures in resisting dynamic loadings such as impact or blast. Commonly employed strengthening methods involve applying compressive or tensile strengthening to the top and bottom surfaces of the structure [64–74]. The fibers in the ECC layer not only improve the ductility of the layer but also increase its energy absorption capacity. As a strengthening material, ECC not only satisfies the durability requirements of the structure but also reduces the damage caused by the impact or blast loadings, which makes it an ideal choice for dynamic strengthening applications.

The addition of an ECC layer can significantly enhance the strength, ductility, and deformation capacity of the member, while also mitigating secondary damage caused by impact fragments. When the ECC is applied to the impacted side of the specimen, it can effectively absorb impact energy, reduce the surface damage caused by the impact, and prevent brittle damage by compression on the impacted side [66,67]. On the other hand, when the ECC layer is positioned on the tensile side, it helps reduce the bottom tensile cracks caused by impact load. The ECC layer on the tensile side undergoes extensive micro-cracking before reaching failure. With the presence of fiber bridging, it can absorb a large amount of energy, thereby avoiding instantaneous major cracks leading to directly brittle failure of the specimen [64–67].

When ECC layer strengthening is applied to masonry, it exhibits excellent strengthening effects on impact resistance. In a study conducted by Pourfalah et al. [59], masonry beams consisting of 10 brick stacks were strengthened using an ECC layer. The addition of the ECC layer significantly enhanced the impact resistance capacity of the masonry member, preventing sudden collapse failure of the specimens. A comparison between specimens strengthened with both top and bottom ECC layers and those with only the bottom layer revealed that the former exhibited higher structural integrity after experiencing multiple impacts. The ECC layer strengthened at the top absorbed each impact energy, redistributed the impact load, prevented cracks in the masonry blocks below, and caused less damage to the ECC at the bottom. The study also observed that under the influence of multiple impacts, cracks are formed in the mid-span brick joint area and extended to the bottom ECC layer, while the ECC layer only forms microcracks below the joint area. As the number of impacts increased, the cracks gradually became denser and wider until eventual failure. In contrast, no visible cracks were found in the ECC layer in the non-brick joints area, indicating that the ductility of the ECC layer was not fully utilized. In order to improve the utilization of the ECC layer, Pourfalah et al. [65] further investigated and discovered that

partially bonded ECC layer specimens exhibited a more uniform crack development at the bottom, thereby dissipating energy more effectively.

ECC strengthening also shows remarkable effects in improving the impact resistance of RC members subject to impact loading. Mahmoud et al. [66,67] demonstrated that RC slabs strengthened with ECC exhibited higher impact resistance compared to unstrengthened slabs. The specimens strengthened on the tensile side in both static and impact conditions showed higher strength and smaller mid-span deflection than those strengthened on the compressive side. In addition, the treatment method of the interface between ECC and concrete played a crucial role in the impact resistance of the structure. Surface roughening with epoxy resin bonding at the bottom effectively improved the impact resistance of ECC-strengthened specimens, but the interface treatment had little effect on the damage pattern of the specimens. Habel and Gauvreau [68] conducted drop hammer tests of ECC-strengthened RC beams with three-point bending or cantilever loading schemes. The ECC layer at the top of the beams was subject to either compressive or tensile stress. The ECC layer did not break, peel or crack during the impact process. And the impact force was uniformly distributed on the upper surface of the structure through the strengthening layer, which reduced the width of cracks during the impact process. In numerical simulations by Wu et al. [69], pickup trucks impacting high strength strain-hardening cementitious composite (HS-SHCC)-strengthened RC barriers were analyzed. The researchers concluded that the back-side strengthening was more effective than the impact surface strengthening. They also noticed that the HS-SHCC layer exhibited high resistance after the peak impact force, dissipated more energy, and reduced the overall damage to the barriers.

There have been relatively few blast resistance tests conducted on ECC-strengthened members. Research conducted by Adhikary et al. [72] demonstrated that RC slabs strengthened with SHCC exhibited lower peak displacement and residual displacement compared to unstrengthened slabs. Moreover, for members with the same thickness of the strengthening layer, slabs strengthened on both sides performed better than those strengthened on the back side only. Liao et al. [73,74] conducted experiments and simulations of strengthened ultra-high ductility concrete and ultra-high performance concrete (UHDC–UHPC) composite slabs subjected to close blast loading. Due to the ultra-high compressive strength and stiffness of the UHPC panels, there was almost no damage to the UHPC on the front side, and only multiple microcracks were observed in the UHDC on the back side under close blast loading, which indicates the excellent blast resistance of the UHDC–UHPC composite slabs.

3.2.2. Dynamic Performance of Members Strengthened by External FRP

Indeed, FRP is also an effective method for enhancing the dynamic properties of a member. One commonly used form of strengthening is to bond FRP to the surface of a member with an epoxy resin to enhance the flexural or shear capacity of the member [3–5]. Numerous studies have shown that FRP strengthening effectively enhances the impact resistance of RC beams, reduces the maximum mid-span deflection, and minimizes damage to the beams [13,17,18,75–78].

Tests conducted by Pham and Hao [17,18] have indicated that FRP-strengthened beams exhibit early peeling damage under impact loading, with the peeling strains usually smaller than those observed in static tests. End anchorage is an effective method recommended by many codes and researchers to prevent early peeling of externally attached FRPs under impact loading [75,76]. Pham and Hao [18] conducted experimental research to prevent FRP peeling by constraining longitudinal FRPs with U-shaped wraps under impact loading. The results indicated that transverse restraint could not completely prevent the occurrence of FRP peeling, but it effectively improved the load-carrying capacity of the longitudinal FRP strips. Similarly, an experiment by Fujikake et al. [77] demonstrated that attaching CFRP strips to the ends of RC beams could prevent the peeling of the bottom CFRP plates. Notably, CFRP-strengthened beams with steel plates and bolts as end anchors could withstand higher impact loads with more pronounced strengthening effects. Ye et al. [16]

found that the dynamic peeling process of FRP under impact loads generates large impact forces on the end anchors, and anchors designed based on static forces may be damaged under impact loads. In addition, Liu et al. [13,78] demonstrated that RC beams without stirrups wrapped with CFRP strips were also effective in reducing deflection and damage. Experiments by Pham et al. [79] on BFRP-strengthened beams demonstrated that beams strengthened with partial U-wraps had similar impact resistance and were more economical than those strengthened with full-span U-wraps.

In summary, the premature peeling damage of the FRP–concrete interface hinders the satisfactory effect of using FRP for strengthening RC beams under impact loading. This limitation significantly restricts the strengthening of the impact energy dissipation capacity of the beams.

3.2.3. Dynamic Performance of ECC–FRP Enhanced Members

Researchers have extensively studied the quasi-static performances of ECC and FRP composite strengthened members. However, fewer investigations have been conducted of their dynamic performance. Static loading research has shown that the composite strengthening of ECC and FRP significantly improves the load-carrying capacity, deformation capacity, and energy dissipation capacity of the members. Notably, ECC demonstrates excellent application potential in structural strengthening under dynamic loading, as it outperforms static loading under dynamic tensile conditions [37–48]. Furthermore, ECC and FRP exhibit high cooperative working ability under static conditions [19,22–25,54]. Therefore, some researchers have begun investigating the performance of ECC and FRP composite strengthened members under dynamic loading conditions [26–29,80–82].

Furthermore, Si et al. [29] investigated the dynamic behaviors of RC beams strengthened at the bottom with ECC–CFRP grid composites. The impact resistance of the strengthened beams was significantly improved under impact loading. Additionally, the load-carrying capacity, ductility, and energy dissipation capacity were enhanced. The development of cracks in the tensile areas was effectively inhibited, preventing the occurrence of brittle damage caused by excessive crack development in RC beams. Furthermore, increasing the ECC thickness and PE fiber content in ECC contributed to an improved bearing capacity of the beam and reduced mid-span displacement. However, when the number of CFRP layers increases, uneven casting of ECC may occur, leading to a weakening of the strengthening effect. It was also discovered that the strengthening effect of single-layer CFRP grids was similar to that of CFRP sheets.

Moreover, Zhou et al. [26] investigated the dynamic behavior of ECC–FRP strengthened RC columns. They conducted scaled tests on truck-impacted bridge pier columns, which were confined with 10 mm thickness of ECC embedded with a layer of CFRP grid. These columns were then compared with unstrengthened columns and columns strengthened with ECC only. The research indicated that the composite strengthening configuration significantly improved the shear carrying capacity of RC columns, restricted the development of shear cracks, and notably reduced the lateral displacement of the strengthened columns, even transforming the shear damage into the overall damage at the column foot. However, when the shear failure is transformed into the overall failure caused by the damage at the column foot, increasing the use of CFRP or ECC had little effect on the displacement of the confined column. Zhou et al. [26–28] also conducted numerical simulation of the test using LS-DYNA. The analysis indicated that ECC could increase the peak impact force, but the CFRP grid had minimal effect on the peak impact force. Furthermore, the scaled-down model was extended to simulate the actual situation. It was discovered that as the impact velocity and force increased, the peak shear force continuously grew larger and approached a constant value. This constant value could be considered as the shear carrying capacity at complete shear damage. In addition, the composite strengthening reduced the tensile stress in the column longitudinal bars of the column and inhibited the development of bending cracks. The CFRP grids worked in conjunction with the stirrup reinforcement to improve the shear performance.

Due to the limited research directly investigating the dynamic performance of composite strengthened specimens, this paper also summarizes the quasi-static test results for composite strengthened specimens, focusing on their deformation and energy dissipation capacity. Zhou et al. [80,81] investigated the seismic strengthening of corroded columns in a coastal environment. They discovered that at 10% corrosion rate, the load-carrying capacity, deformation capacity, and energy dissipation capacity of the enhanced repaired columns were superior to those of uncorroded columns. Lim et al. [82] conducted research on the retrofitting of strengthened concrete beam–column joints using CFRP grids with ECC or high-strength mortar, as shown in Figure 7. After the cyclic loading at the top of the column, it was observed that the total dissipated energy of all retrofitted specimens exceeded that of the specimens without retrofitting. The "W" strengthened ECC retrofitted specimens dissipated the highest energy. In addition, the ultimate strength and the displacement corresponding to the maximum load were improved by 6.99~23.47% and 9.62~177.56% respectively according to the different retrofitting methods. The deformation capacity was significantly enhanced. Among the various retrofitting methods, the "W" type retrofitting using CFRP grids with ECC exhibited the most effective retrofitting effect. However, it was noted that due to the difference in ultimate strain between CFRP grids and concrete, CFRP grids did not completely utilize their potential.

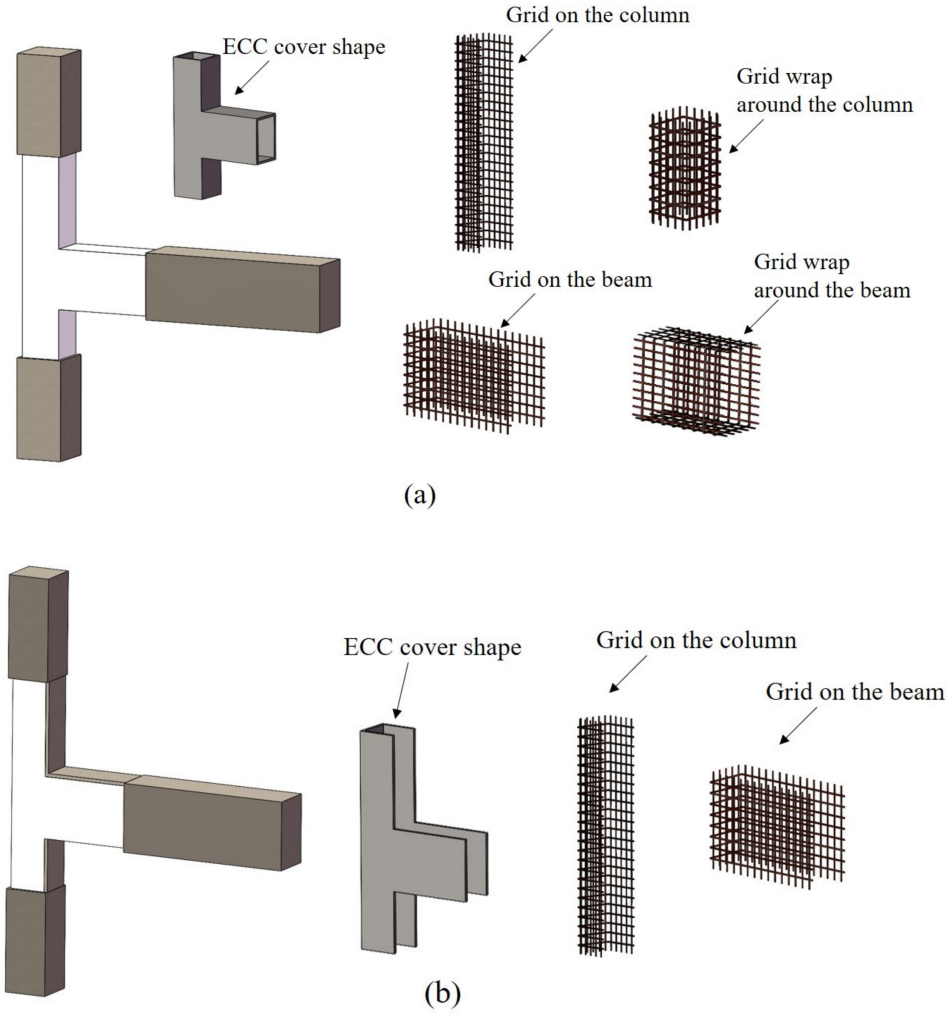


Figure 7. Schematic drawing of "W" and "S" type joint retrofit: (**a**) Schematic drawing of type "W" retrofitting specimen with CFRP grid configuration; (**b**) schematic drawing of type "S" retrofitting specimen with CFRP grid configuration [82].

In conclusion, the strengthening of ECC–FRP grid composites demonstrates significant potential for both research and practical applications. It effectively improves the load-carrying capacity, deformation capacity, and energy dissipation capacity of structural members, thereby providing better resistance against dynamic loading damage caused by various dynamic disasters. Despite its promising benefits, there remains a scarcity of relevant research in this area. To ensure the reliability and applicability of ECC–FRP grid composite strengthening, further investigations by researchers are necessary. These studies can involve experimental testing, numerical simulations, and analytical modeling to assess the behavior of the material under various loading conditions and environmental exposures. In addition to validating its reliability, researchers can also focus on exploring the effects of different factors on the composite strengthening effect. These factors may include the type, orientation, and volume fraction of fibers used, the type of matrix material employed, and the geometry of the grid reinforcement. In summary, the research and development of ECC–FRP grid composites represent a promising avenue for advancing construction materials and engineering practices. However, to harness their full potential, further investigations and exploration of key factors are essential.

4. Conclusions

This paper presents a comprehensive review of the research progress on ECC and its composite with FRP at both material and member levels. The following are some summaries:

The performance of ECC is influenced by various factors, including fiber type, fiber size, fiber content, matrix composition, etc. Notably, ECC exhibits a significant strain-rate effect, leading to considerable variation in performance at high strain rates. Typically, the dynamic performance of the ECC is more significantly improved at high strain rates. However, the experimental results in previous studies present large scatterness, and formulas quantitatively describing strain-rate effects of key indicators, including ultimate strength and strain, have not been proposed yet.

Under static loadings, the ECC–FRP composite demonstrates excellent cooperative working ability. ECC contributes to crack inhibition and compression resistance, while FRP enhances tensile strength and stiffness, resulting in outstanding tensile properties, ductility, and crack control capability, which enhanced the overall performance of the structure. However, there is a lack of research on the properties of ECC–FRP grid composites under dynamic loading. Further investigations and practical experiences are crucial for improving the design and application of such composites.

Due to the high ductility and multiple microcrack characteristics, ECC members exhibit excellent deformation and exceptional energy absorption capabilities when subjected to impact loading. Moreover, a coordinated deformation between ECC and rebars can be achieved. This results in the extension of plastic yielding within the longer reinforcement section, subsequently restricting crack propagation. By reasonably adjusting the material composition of ECC, it is possible to significantly enhance the impact resistance of ECC members.

For ECC-strengthened members under dynamic loading, the fibers in ECC not only improve the overall ductility but also increase its energy absorption capacity. At the same time, the ECC layer can play a role in limiting the occurrence of primary cracks, which may result in the brittle failure of the member. And an ECC layer can mitigate secondary damage caused by impact fragments. As a strengthening material, ECC meets the durability requirements of the structure and reduces the damage caused by dynamic loading.

FRP strengthening effectively improves the impact resistance of members and reduces the damage of members. However, it is important to note that proper anchoring measures are necessary to prevent potential debonding issues that may compromise its strengthening effects.

ECC–FRP grid strengthening presents a promising approach for significantly enhancing the load-bearing capacity, deformation capacity, and energy dissipation capacity of

RC members. While there are encouraging indications of its potential application under dynamic loading, further research is required to ensure its effectiveness and reliability.

Author Contributions: Conceptualization, D.Z.; methodology, D.Z.; investigation, D.Z. and B.C.; resources, J.S.; writing—original draft preparation, D.Z. and B.C.; writing—review and editing, D.Z. and J.S.; supervision, D.Z. and J.S.; funding acquisition, D.Z. All authors have read and agreed to the published version of the manuscript.

Funding: The research work described herein was funded by the National Key Research and Development Program (Grant No. 2021YFB2601000), the National Natural Science Foundation of China (Grant No. 52090084), and the Guangdong Basic and Applied Basic Research Foundation (No. 2023A1515010224). This financial support is gratefully acknowledged.

Data Availability Statement: The data presented in this study are available on request from the corresponding author. The data are not publicly available due to privacy restrictions.

Conflicts of Interest: The authors declare no conflict of interest.

References

1. Zhao, D.; Yi, W.; Kunnath, S.K. Shear Mechanisms in Reinforced Concrete Beams under Impact Loading. *J. Struct. Eng.* **2017**, *143*, 04017089. [CrossRef]
2. Zhao, D.; Huang, Y.; Chen, X.; Han, K.; Chen, C.; Zhao, X.; Chen, W. Numerical investigations on dynamic responses of subway segmental tunnel lining structures under internal blasts. *Tunneling Undergr. Space Technol.* **2023**, *135*, 105058. [CrossRef]
3. Zhou, Y.; Ye, Z.; Zhao, D.; Huang, Z.; Yang, L. Static and multi-impact performances of RC beams strengthened with large rupture-strain FRP composites. *Compos. Struct.* **2023**, *316*, 117053. [CrossRef]
4. Buth, C.E.; Williams, W.F.; Brackin, M.S.; Lord, D.; Geedipally, S.R.; Abu-Odeh, A.Y. *Analysis of Large Truck Collisions with Bridge Piers: Phase 1. Report of Guidelines for Designing Bridge Piers and Abutments for Vehicle Collisions*; Texas Transportation Institute the Texas A&M University System: College Station, TX, USA, 2010.
5. Tachibana, S.; Masuya, H.; Nakamura, S. Performance based design of reinforced concrete beams under impact. *Nat. Hazards Earth Syst. Sci.* **2010**, *10*, 1069–1078. [CrossRef]
6. Li, V.C. *Engineered Cementitious Composites (ECC): Bendable Concrete for Sustainable and Resilient Infrastructure*; Springer: Berlin/Heidelberg, Germany, 2019.
7. Li, V.C.; Wang, S.; Wu, C. Tensile strain-hardening behavior of polyvinyl alcohol engineered cementitious composite (PVA-ECC). *ACI Mater. J.* **2001**, *98*, 483–492.
8. Xu, S.; Chen, B.; Li, Q.; Zhou, F.; Yin, X.; Jiang, X.; Wu, P. Experimental and numerical investigations on ultra-high toughness cementitious composite slabs subjected to close-in blast loadings. *Cem. Concr. Compos.* **2022**, *126*, 104339. [CrossRef]
9. Li, Q.; Chen, B.; Xu, S.; Zhou, F.; Yin, X.; Jiang, X.; Wu, P. Experiment and numerical investigations of ultra-high toughness cementitious composite slabs under contact explosions. *Int. J. Impact Eng.* **2022**, *159*, 104033. [CrossRef]
10. Nam, J.; Kim, H.; Kim, G. Experimental Investigation on the Blast Resistance of Fiber-Reinforced Cementitious Composite Panels Subjected to Contact Explosions. *Int. J. Concr. Struct. Mater.* **2017**, *11*, 29–43. [CrossRef]
11. Yang, E.; Li, V.C. Tailoring engineered cementitious composites for impact resistance. *Cem. Concr. Res.* **2012**, *42*, 1066–1071. [CrossRef]
12. Zhang, J.; Maalej, M.; Quek, S.T. Performance of Hybrid-Fiber ECC Blast/Shelter Panels Subjected to Drop Weight Impact. *J. Mater. Civ. Eng.* **2007**, *19*, 855–863. [CrossRef]
13. Liu, T.; Xiao, Y. Impact Behavior of CFRP-Strip Wrapped RC Beams without Stirrups. *J. Compos. Constr. (ASCE)* **2017**, *21*, 04017035. [CrossRef]
14. Del Zoppo, M.; Di Ludovico, M.; Balsamo, A.; Prota, A.; Manfredi, G. FRP for seismic strengthening of shear controlled RC columns: Experience from earthquakes and experimental analysis. *Compos. Part B Eng.* **2017**, *129*, 47–57. [CrossRef]
15. Zhou, A.; Qin, R.; Feo, L.; Penna, R.; Lau, D. Investigation on interfacial defect criticality of FRP-bonded concrete beams. *Compos. Part B Eng.* **2017**, *113*, 80–90. [CrossRef]
16. Ye, Z.; Zhao, D.; Sui, L.; Huang, Z.; Zhou, X. Behaviors of Large-Rupture-Strain Fiber-Reinforced Polymer Strengthened Reinforced Concrete Beams Under Static and Impact Loads. *Front. Mater.* **2020**, *7*, 578749. [CrossRef]
17. Pham, T.M.; Hao, H. Impact Behavior of FRP-Strengthened RC Beams without Stirrups. *J. Compos. Constr.* **2016**, *20*, 04016011. [CrossRef]
18. Pham, T.M.; Hao, H. Behavior of FRP Strengthened RC Beams under Static and Impact Loads. *Int. J. Prot. Struct.* **2016**, *8*, 3–24. [CrossRef]
19. Jiang, J.; Jiang, C.; Li, B.; Feng, P. Bond behavior of basalt textile meshes in ultra-high ductility cementitious composites. *Compos. Part B Eng.* **2019**, *174*, 107022. [CrossRef]
20. Zheng, A.; Liu, Z.; Li, F.; Li, S. Experimental investigation of corrosion-damaged RC beams strengthened in flexure with FRP grid-reinforced ECC matrix composites. *Eng. Struct.* **2021**, *244*, 112779. [CrossRef]

21. Zheng, Y.; Wang, W.; Brigham, J.C. Flexural behaviour of reinforced concrete beams strengthened with a composite reinforcement layer: BFRP grid and ECC. *Constr. Build. Mater.* **2016**, *115*, 424–437. [CrossRef]
22. Zhu, Z.; Wang, W.; Harries, K.A.; Zheng, Y. Uniaxial Tensile Stress–Strain Behavior of Carbon-Fiber Grid–Reinforced Engineered Cementitious Composites. *J. Compos. Constr.* **2018**, *22*, 04018057. [CrossRef]
23. Zheng, Y.; Wang, W.; Mosalam, K.M.; Zhu, Z. Mechanical behavior of ultra-high toughness cementitious composite strengthened with Fiber Reinforced Polymer grid. *Compos. Struct.* **2018**, *184*, 1–10. [CrossRef]
24. Li, B.; Xiong, H.; Jiang, J.; Dou, X. Tensile behavior of basalt textile grid reinforced Engineering Cementitious Composite. *Compos. Part B Eng.* **2019**, *156*, 185–200. [CrossRef]
25. Gong, T.; Ahmed, A.H.; Curosu, I.; Mechtcherine, V. Tensile behavior of hybrid fiber reinforced composites made of strain-hardening cement-based composites (SHCC) and carbon textile. *Constr. Build. Mater.* **2020**, *262*, 120913. [CrossRef]
26. Zhou, C.; Wang, W.; Zheng, Y.; Liu, X.; Cao, H.; Hui, Y. Dynamic behavior of RC columns confined with CFRP grid-reinforced ECC subjected to lateral low-velocity impact. *Int. J. Impact Eng.* **2023**, *172*, 104402. [CrossRef]
27. Zhou, C.; Xie, Y.; Wang, W.; Zheng, Y. Performance-based design for improving impact resistance of RC bridge piers with CFRP grid-reinforced ECC. *Eng. Struct.* **2023**, *275*, 115217. [CrossRef]
28. Zhou, C.; Wang, W.; Zheng, Y.; Cheng, Y.; Wu, Z. Response and shear mechanism of RC bridge piers confined with CFRP grid-reinforced ECC subjected to truck collision. *Eng. Fail. Anal.* **2023**, *143*, 106882. [CrossRef]
29. Si, Z.; Liu, F.; Pan, J.; Dong, H. Research on Impact Resistance of Reinforced Concrete Beams Strengthened with Carbon Fiber Reinforced Polymer Grid and Engineered Cementitious Composites. *Polymers* **2022**, *14*, 1951. [CrossRef]
30. Li, Q.; Zhao, X.; Xu, S.; Gao, X. Influence of steel fiber on dynamic compressive behavior of hybrid fiber ultra high toughness cementitious composites at different strain rates. *Constr. Build. Mater.* **2016**, *125*, 490–500. [CrossRef]
31. Zhao, X.; Xu, S.; Li, Q.; Chen, B. Coupled effects of high temperature and strain rate on compressive properties of hybrid fiber UHTCC. *Mater. Struct.* **2019**, *52*, 92. [CrossRef]
32. Kai, M.F.; Xiao, Y.; Shuai, X.L.; Ye, G. Compressive Behavior of Engineered Cementitious Composites under High Strain-Rate Loading. *J. Mater. Civ. Eng.* **2017**, *29*, 04016254. [CrossRef]
33. Chen, Z.; Yang, Y.; Yao, Y. Quasi-static and dynamic compressive mechanical properties of engineered cementitious composite incorporating ground granulated blast furnace slag. *Mater. Des.* **2013**, *44*, 500–508. [CrossRef]
34. Wang, S.; Le, H.T.N.; Poh, L.H.; Quek, S.T.; Zhang, M.H. Effect of high strain rate on compressive behavior of strain-hardening cement composite in comparison to that of ordinary fiber-reinforced concrete. *Constr. Build. Mater.* **2017**, *136*, 31–43. [CrossRef]
35. Zhang, N.; Zhou, J.; Ma, G. Dynamic Properties of Strain-Hardening Cementitious Composite Reinforced with Basalt and Steel Fibers. *Int. J. Concr. Struct. Mater.* **2020**, *14*, 44. [CrossRef]
36. Chen, Z.; Yang, Y.; Yao, Y. Impact properties of engineered cementitious composites with high volume fly ash using SHPB test. *J. Wuhan Univ. Technol.-Mater. Sci. Ed* **2021**, *27*, 590–596. [CrossRef]
37. Mechtcherine, V.; de Andrade Silva, F.; Butler, M.; Zhu, D.; Mobasher, B.; Gao, S.L.; Mäder, E. Behaviour of Strain-Hardening Cement-Based Composites Under High Strain Rates. *J. Adv. Concr. Technol.* **2011**, *9*, 51–62. [CrossRef]
38. Curosu, I.; Mechtcherine, V.; Forni, D.; Cadoni, E. Performance of various strain-hardening cement-based composites (SHCC) subject to uniaxial impact tensile loading. *Cem. Concr. Res.* **2017**, *102*, 16–28. [CrossRef]
39. Yu, K.; Dai, J.; Lu, Z.; Poon, C.S. Rate-dependent tensile properties of ultra-high performance engineered cementitious composites (UHP-ECC). *Cem. Concr. Compos.* **2018**, *93*, 218–234. [CrossRef]
40. Ranade, R.; Li, V.C.; Heard, W.F. Tensile Rate Effects in High Strength-High Ductility Concrete. *Cem. Concr. Res.* **2015**, *68*, 94–104. [CrossRef]
41. Maalej, M.; Quek, S.T.; Zhang, J. Behavior of Hybrid-Fiber Engineered Cementitious Composites Subjected to Dynamic Tensile Loading and Projectile Impact. *J. Mater. Civ. Eng.* **2005**, *17*, 143–152. [CrossRef]
42. Yao, Y.; Silva, F.A.; Butler, M.; Mechtcherine, V.; Mobasher, B. Failure Localization and Correlation of High-Speed Tension and Impact Tests of Strain-Hardening Cement-Based Composites. *J. Mater. Civ. Eng.* **2017**, *29*, 04017212. [CrossRef]
43. Zhao, X.; Zou, B.; Wang, M.; Li, H.; Lou, Z. Influence of free water on dynamic tensile behavior of ultra-high toughness cementitious composites. *Constr. Build. Mater.* **2021**, *269*, 121295. [CrossRef]
44. Yang, E.; Li, V.C. Strain-rate effects on the tensile behavior of strain-hardening cementitious composites. *Constr. Build. Mater.* **2014**, *52*, 96–104. [CrossRef]
45. Zhao, X.; Li, Q.; Xu, S. Contribution of steel fiber on the dynamic tensile properties of hybrid fiber ultra high toughness cementitious composites using Brazilian test. *Constr. Build. Mater.* **2020**, *246*, 118416. [CrossRef]
46. Chen, M.; Wang, Y.; Zhang, T.; Zhang, M. Behaviour of structural engineered cementitious composites under dynamic tensile loading and elevated temperatures. *Eng. Struct.* **2023**, *280*, 115739. [CrossRef]
47. Yang, G.; Dong, Z.; Bi, J.; Zhao, K.; Li, F. Experimental study on the dynamic splitting tensile properties of polyvinyl-alcohol-fiber-reinforced cementitious composites. *Constr. Build. Mater.* **2023**, *383*, 131233. [CrossRef]
48. Curosu, I.; Liebscher, M.; Mechtcherine, V.; Bellmann, C. Tensile behavior of high-strength strain-hardening cement-based composites (HS-SHCC) made with high-performance polyethylene, aramid and PBO fibers. *Cem. Concr. Res.* **2017**, *98*, 71–81. [CrossRef]
49. De Belie, N.; Gruyaert, E.; Al-Tabbaa, A.; Antonaci, P.; Baera, C.; Bajare, D.; Darquennes, A.; Davies, R.; Ferrara, L.; Jefferson, T. A Review of Self-Healing Concrete for Damage Management of Structures. *Adv. Mater. Interfaces* **2018**, *5*, 1800074. [CrossRef]

50. Amir, S.; Rebecca, G.; Filippo, G. Is concrete healing really efficient? A review. *Constr. Build. Mater.* **2019**, *205*, 257–273.
51. Hossain, M.R.; Sultana, R.; Patwary, M.M.; Khunga, N.; Sharma, P.; Shaker, S.J. Self-healing concrete for sustainable buildings. A review. *Environ. Chem. Lett.* **2022**, *20*, 1265–1273. [CrossRef]
52. Guo, W.; Bao, J.; Zhang, P.; Yang, J.; Guo, D.; Tian, Y. Self-healing behavior of strain-hardening cementitious composites with MgO-type expansive agent after drop weight impact loading. *Constr. Build. Mater.* **2023**, *366*, 130235. [CrossRef]
53. Tang, Z.; Cao, B.; Litina, C.; Afroughsabet, V.; Vlachakis, C.; Al-Tabbaa, A. Development of novel self-healing strain-hardening cementitious composites (SH2CC) for dynamic cyclic loading conditions using mineral and polymer admixtures. *Cem. Concr. Compos.* **2023**, *142*, 105172. [CrossRef]
54. Deng, L.; Lei, L.; Lai, S.; Liao, L.; Zhou, Z. Experimental Study on the Axial Tensile Properties of FRP Grid-Reinforced ECC Composites. *Materials* **2021**, *14*, 3936. [CrossRef]
55. Zheng, Y. Experiment and Calculation Method Research on Reinforced Concrete (RC) Beams Strengthened with the Composite of FRP Grid and ECC. Ph.D. Thesis, Southeast University, Nanjing, China, 2018.
56. Deng, L.; Li, T.; Zhong, M.; Liao, L.; Li, H. Bond Stress–Slip Model of BFRP Grid to ECC. *Materials* **2022**, *15*, 7965. [CrossRef] [PubMed]
57. Baral, K.; Tatar, J.; Zhang, Q. High-Performance Impact-Resistant Concrete Mixture for Transportation Infrastructure Applications. *Transp. Res. Rec. J. Transp. Res. Board* **2019**, *2673*, 628–635. [CrossRef]
58. Anil, Ö.; Durucan, C.; Erdem, R.T.; Yorgancilar, M.A. Experimental and numerical investigation of reinforced concrete beams with variable material properties under impact loading. *Constr. Build. Mater.* **2016**, *125*, 94–104. [CrossRef]
59. Ranade, R.; Li, V.C.; Heard, W.F.; Williams, B.A. Impact resistance of high strength-high ductility concrete. *Cem. Concr. Res.* **2017**, *98*, 24–35. [CrossRef]
60. Yıldırım, G.; Khiavi, F.E.; Anıl, Ö.; Şahin, O.; Şahmaran, M.; Erdem, R.T. Performance of engineered cementitious composites under drop-weight impact: Effect of different mixture parameters. *Struct. Concr.* **2019**, *21*, 1051–1070. [CrossRef]
61. Zhang, Z.; Qin, F.; Ma, H.; Xu, L. Tailoring an impact resistant engineered cementitious composite (ECC) by incorporation of crumb rubber. *Constr. Build. Mater.* **2020**, *262*, 120116. [CrossRef]
62. Qi, B.; Kong, Q.; Qian, H.; Patil, D.; Lim, I.; Li, M.; Song, G. Study of Impact Damage in PVA-ECC Beam under Low-Velocity Impact Loading Using Piezoceramic Transducers and PVDF Thin-Film Transducers. *Sensors* **2018**, *18*, 671. [CrossRef]
63. Lu, C.; Yu, J.; Leung, C.K.Y. Tensile performance and impact resistance of Strain Hardening Cementitious Composites (SHCC) with recycled fibers. *Constr. Build. Mater.* **2018**, *171*, 566–576. [CrossRef]
64. Pourfalah, S.; Cotsovos, D.M.; Suryanto, B.; Moatamedi, M. Out-of-plane behaviour of masonry specimens strengthened with ECC under impact loading. *Eng. Struct.* **2018**, *173*, 1002–1018. [CrossRef]
65. Pourfalah, S.; Cotsovos, D.M. Enhancing the out-of-plane behaviour of unreinforced masonry walls under impact loading through the use of partially bonded layers of engineered cementitious composite. *Int. J. Prot. Struct.* **2019**, *11*, 209–234. [CrossRef]
66. Mahmoud, M.H.; Afefy, H.M.; Baraghith, A.T.; Elnagar, A.B. Impact and static behavior of strain-hardening cementitious composites–strengthened reinforced concrete slabs. *Adv. Struct. Eng.* **2020**, *23*, 1614–1628. [CrossRef]
67. Elnagar, A.B.; Afefy, H.M.; Baraghith, A.T.; Mahmoud, M.H. Experimental and numerical investigations on the impact resistance of SHCC-strengthened RC slabs subjected to drop weight loading. *Constr. Build. Mater.* **2019**, *229*, 116866. [CrossRef]
68. Habel, K.; Gauvreau, P. Behavior of Reinforced and Posttensioned Concrete Members with a UHPFRC Overlay under Impact Loading. *J. Struct. Eng.* **2009**, *135*, 292–300. [CrossRef]
69. Wu, C.; Mahmoud, M.; Hou, C.; Topa, A. Study on the impact performance of RC fences strengthened with high strength strain-hardening cementitious composites. *Structures* **2022**, *41*, 349–364. [CrossRef]
70. Leblouba, M.; Altoubat, S.; Karzad, A.S.; Maalej, M.; Barakat, S.; Metawa, A. Impact response and endurance of unreinforced masonry walls strengthened with cement-based composites. *Structures* **2022**, *36*, 262–279. [CrossRef]
71. Batran, T.Z.; Ismail, M.K.; Hassan, A.A.A. Behavior of novel hybrid lightweight concrete composites under drop-weight impact loading. *Structures* **2021**, *34*, 2789–2800. [CrossRef]
72. Adhikary, S.D.; Chandra, L.R.; Christian, A.; Ong, K.C.G. SHCC-strengthened RC panels under near-field explosions. *Constr. Build. Mater.* **2018**, *183*, 675–692. [CrossRef]
73. Liao, Q.; Yu, J.; Xie, X.; Ye, J.; Jiang, F. Experimental study of reinforced UHDC-UHPC panels under close-in blast loading. *J. Build. Eng.* **2022**, *46*, 103498. [CrossRef]
74. Liao, Q.; Xie, X.; Yu, J. Numerical investigation on dynamic performance of reinforced ultra-high ductile concrete-ultra-high performance concrete panel under explosion. *Struct. Concr.* **2022**, *23*, 3601–3615. [CrossRef]
75. Zhou, C.; Ren, D.; Liu, J.; He, X. Tests of RC continuous T-beams shear-strengthened with CFRP U-strips around rods through eye bolts penetrating beam flange. *J. Build. Struct.* **2020**, *41*, 156–164.
76. ACI Committee 440. *Guide for the Design and Construction of Externally Bonded FRP Systems for Strengthening Concrete Structures*; American Concrete Institute: Farmington Hills, MI, USA, 2008.
77. Fujikake, K.; Soeum, S.; Matsui, T. CFRP strengthened RC beams subjected to impact loading. *Procedia Eng.* **2017**, *210*, 173–181. [CrossRef]
78. Liu, T.; Kang, H.-K.T.; Nghiem, A.; Xiao, Y. Impact Testing of Reinforced Concrete Members Shear-Strengthened with Fiber-Reinforced Polymer Wraps. *ACI Struct. J.* **2020**, *117*, 297–310.

79. Pham, T.M.; Chen, W.; Elchalakani, M.; Karrech, A.; Hao, H. Experimental investigation on lightweight rubberized concrete beams strengthened with BFRP sheets subjected to impact loads. *Eng. Struct.* **2020**, *205*, 110095. [CrossRef]
80. Zhou, Y.; Wang, X.; Yuan, F.; Hu, B.; Zhu, Z. Seismic retrofitting of coastal structural columns with steel bars locally corroded to fracture using sprayed ECC overlays and FRP jackets. *Compos. Struct.* **2023**, *307*, 116670. [CrossRef]
81. Zhou, Y.; Wang, X.; Hu, B.; Sui, L.; Yuan, F. Seismic Retrofit of Nonuniformly Corroded Coastal Bridge Piers with FRP and Engineered Cementitious Composite Overlays. *J. Compos. Constr.* **2022**, *27*, 04022088. [CrossRef]
82. Lim, C.; Jeong, Y.; Kim, J.; Kwon, M. Experimental study of reinforced concrete beam-column joint retrofitted by CFRP grid with ECC and high strength mortar. *Constr. Build. Mater.* **2022**, *340*, 127694. [CrossRef]

Disclaimer/Publisher's Note: The statements, opinions and data contained in all publications are solely those of the individual author(s) and contributor(s) and not of MDPI and/or the editor(s). MDPI and/or the editor(s) disclaim responsibility for any injury to people or property resulting from any ideas, methods, instructions or products referred to in the content.